Preprints of the 21st IFAC World Congress (Virtual)
Berlin, Germany, July 12-17, 2020

Decentralized LQG Control for Adaptive High-Rise Structures

Alexander Warsewa * **Julia Laura Wagner** * **Michael Böhm** *
Oliver Sawodny * **Cristina Tarín** *

* *Institute for System Dynamics, Waldburgstr. 19, DE-70563 Stuttgart (e-mail: warsewa@isys.uni-stuttgart.de).*

Abstract: Adaptivity of buildings introduces new challenges and opportunities for both architects and engineers. With the possibility of active load compensation, new types of lightweight structures can be realized. However, those demand suitable control engineering methods to ensure safe and robust control. In this contribution, we introduce an approach for decentralized linear quadratic Gaussian (LQG) control of adaptive structures. Many state of the art methods in decentralized structural control focus on damping the response of substructures that are either derived by decomposition of a global finite element (FE) model or later assembled to form a complete structure. In contrast, we derive local models by means of model order reduction techniques which allows for fully decentralized control without the need to communicate states or estimate interaction forces. We demonstrate the decentralized control of local subsystems for an adaptive structures demonstrator building in simulations. Performance and energy demand are found to be comparable to a centralized controller which makes the presented approach well suitable for application. Monte Carlo simulations with both varying model parameters and system eigenvalues were conducted to analyze the robustness of the decentralized LQG controllers.

Keywords: Adaptive structures; structural dynamics; state estimation; decentralized control; model order reduction

1. INTRODUCTION

Introducing active load-bearing elements and sensor technology into truss structures leads to *adaptive structures* opening up new possibilities for ultra-lightweight construction. The use of supplemental passive, semi-active or active devices to reduce structural vibrations is not a novel concept as pointed out by e. g. Spencer and Nagarajaiah (2003). A proven, though rarely realized, example of an active device that allows for building relatively lightweight high-rise structures is the active tuned mass damper (ATMD). In the concept of adaptive structures, the actuator is considered an integral part of the truss structure instead of an additional mechanism. This more radical view comes with a higher potential for the reduction of embodied energy associated with the construction of buildings as discussed by Sobek and Teuffel (2001). However, the complexity rises in every phase of the construction process and suitable solutions for both monitoring and control of such structures need to be developed.

Especially tall buildings or structures with a wide span - when equipped with a multitude of sensors and actuators - require the communication of a large amount of data over long distances. Central acquisition and processing of sensor data for real-time control can be both challenging and cost-intensive in such cases. At the same time, failure of the central control unit cannot be tolerated. In view of those issues, decentralized estimation and control approaches are the logical consequence. An early survey on decentralized control approaches for large-scale structures is given in Sandell et al. (1978) and a more recent one with a more general focus on complex systems in Siljak (2011).

Most available work on decentralized structural control focuses on the application of linear quadratic Gaussian (LQG) control to individual substructures. In the substructural controller synthesis method introduced by Su et al. (1995), individual controllers are first designed for each substructure which are later combined via coupling matrices to form a global controller. It is often the case that the dynamics of the assembled system differ significantly from those of the substructures it is composed of which renders this approach suboptimal. Lynch and Law (2002) achieve decentralized control with linear quadratic regulators (LQR) that operate on substructures derived from a decomposition of the dynamic equations in matrix second-order form. This requires that the interactions between subsystems are either small or known to achieve performance comparable to a centralized controller. A similar approach is presented by Lei et al. (2012), where the state estimation problem is also taken into account. The resulting controllers need to communicate their states and observers are charged with the recursive estimation of interaction forces between subsystems. With respect to unknown disturbances, robustness of the latter cannot be easily guaranteed. Bakule et al. (2016) extend the same kind of decentralized LQG approach to account for networked coordination of the subsystem controllers on a higher level. Velocity and displacement feedback for substructural control is shown in Rofooei and Monajemi-

Nezhad (2006) where it is assumed that the dynamic equations can be decoupled by means of a transformation.

In contrast to the aforementioned approaches to decentralized structural control, we propose to use model order reduction techniques to derive local models from a global finite element (FE) representation. This way, fully decentralized LQG control of the resulting subsystems is possible without the need to communicate states or explicitly account for interaction forces between substructures. In Warsewa et al. (2019), we introduced a decentralized and distributed estimation approach for large-scale structures. The models for local observers are obtained by applying a combination of static and dynamic condensation techniques and modal analysis to the global model. Each local observer is able to give an estimate of the global state by inverse transformation. This is potentially advantageous for a coordination of modules in a hierarchical fashion and also for inter-module communication both of which is not within the scope of this publication.

Here, we show the applicability of this approach to the decentralized control problem. For illustration purposes, we use the simulation model of an adaptive structures demonstrator building that is to be built on campus of the University of Stuttgart to present this emerging technology to a broader audience.

The remainder of this contribution begins by introducing the dynamic model of the demonstrator. Modal analysis is employed to obtain a lower order system in modal coordinates for simulation purposes and the derivation of local subsystems from the global model for decentralized control is presented in Sec. 2.4. This is followed in Secs. 3 and 4 by a brief introduction of the filtering and control algorithms employed for both decentralized control and the centralized approaches used for comparison. The performance of the presented decentralized LQG control method is investigated in simulations in Sec. 5 and robustness analysis is conducted by means of Monte Carlo experiments. Concluding remarks are given in Sec. 6.

2. MODELING

To illustrate the application of the methods presented in this contribution to adaptive structures, we consider decentralized control of the aforementioned demonstrator building. In the following section, a dynamic model of the structure is introduced. Modal analysis is employed to obtain a simulation model of lower order. Distribution of a limited number of actuators and sensors on the demonstrator is based on previous work and briefly outlined in Sec. 2.2. In Sec. 2.4, we show the application of the method presented in Warsewa et al. (2019) to obtain local models for individual modules of the demonstrator.

2.1 Adaptive Structure Model

On the left hand side in Fig. 1, a schematic representation of the demonstrator is visible. When considering only the passive structure, the building is composed of four identical modules. For decentralized control, each of the four modules shown on the right hand side of Fig. 1 is controlled independently. Each substructure has three stories, four vertical columns, eight diagonal bracings and

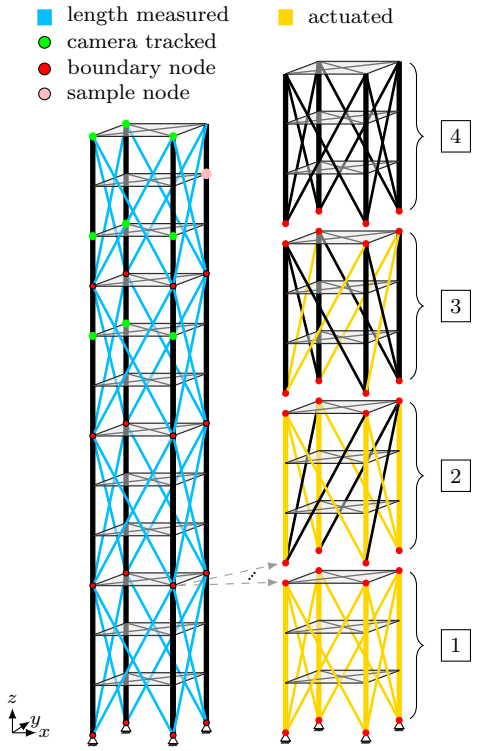

Fig. 1. Schematic drawing of an adaptive high-rise building and its decomposition into four modules with actuators (yellow), elements equipped with strain gauges (blue), camera-tracked nodes (green), boundary nodes (red) and the node for which the x-displacement is plotted in the results section (pink).

twelve horizontal bars. Floor plates are represented by two diagonal links. Geometry and material parameters can be found in Tab. 1. All truss elements are made of structural steel. Vertical columns are modeled as beams whereas all other elements are modeled as links taking only loads in the axial direction. Except for the rotations about the x- and y-axis, the DOFs of the ground nodes are fixed.

Adaptivity is introduced by means of hydraulic actuators connected in parallel to selected vertical columns and diagonals, as described in Wagner et al. (2018). The actuator dynamics are assumed negligible here such that the actuator contribution can be modeled as a force acting on the boundary nodes of an active element.

We obtain the structural dynamics from a finite element model as

$$M\ddot{\boldsymbol{q}}(t) + D\dot{\boldsymbol{q}}(t) + K\boldsymbol{q}(t) = F_u\boldsymbol{u}(t), \quad t > 0, \tag{1}$$

$$\boldsymbol{q}(t=0) = q_0, \quad \dot{\boldsymbol{q}}(t=0) = \boldsymbol{q}_1. \tag{2}$$

Here, $\boldsymbol{q}(t) \in \mathbb{R}^n$ are the structure's DOFs, M and K are the symmetric, positive definite mass and stiffness matrices and F_u is the input matrix that maps the actuator forces $\boldsymbol{u}(t)$ to the DOFs. Rayleigh damping is assumed such that the damping matrix is obtained as a linear combination of M and K

$$D = \alpha_1 M + \alpha_2 K \tag{3}$$

with the damping coefficients α_1 and α_2.

Information on the structural deformation of the demonstrator can be obtained via strain gauge sensors and a

camera system. The latter uses two cameras to track the displacements of a number of emitters mounted to the facade at structural nodes. For details on the measurement principle, refer to Guerra et al. (2019). One camera can measure xz-displacements and the other yz-displacements. In this contribution, we assume that the displacements of nine emitters placed on the upper section of the building can be tracked. The selected nodes are highlighted in green in Fig. 1. This amounts to a total of $m_\mathrm{c} = 24$ displacement signals from the cameras where the z-displacement is measured twice for the emitters captured by both cameras. The length of diagonal bracings is measured by $m_\mathrm{l} = 32$ strain gauges highlighted in blue in Fig. 1.

2.2 Sensor and Actuator Placement

The selection of diagonal bracings for sensor placement is a result of an optimization algorithm developed in previous work. The same method was used to determine the optimal location of the $n_u = 24$ actuators highlighted in yellow in the substructures shown in Fig. 1. In Heidingsfeld et al. (2017), a greedy algorithm is presented that sequentially selects the best position of each actuator using measures derived from the controllability Gramian as an optimality criterion. This method was further extended to optimal actuator placement for compensating static disturbances in Wagner et al. (2018) and adapted to the sensor placement problem using the observability Gramian in Rapp et al. (2017).

2.3 Modal Analysis

We employ modal analysis to reduce the system order by truncation of high-frequency eigenmodes. This reduces numerical problems caused by the stiff nature of the dynamics (1) and increases simulation speed. A detailed treatise of this widely-used technique can be found in e. g. Gawronski (2004).

The solution of (1) without damping and input terms amounts to

$$\boldsymbol{q}(t) = \varphi_i e^{j\omega_i t} \tag{4}$$

with eigenvalues ω_i and the corresponding eigenvectors φ_i. Taking the second derivative of the above, the dynamic equation without damping and external excitation can be reformulated as

$$(K - \omega_i^2 M)\varphi_i = 0, \quad i = 1, 2, \dots n. \tag{5}$$

This equation can be solved for ω_i and the eigenvectors φ_i. Since the latter are not uniquely determined, they are normalized such that $\Phi^\mathrm{T} M \Phi = I$ with $\Phi = [\varphi_1 \ \varphi_2 \ \dots \ \varphi_n]^\mathrm{T}$.

A reduced order model in modal coordinates is then obtained by approximating the vector of DOFs $\boldsymbol{q}(t)$ by a small number of primary eigenmodes

$$\boldsymbol{q}(t) \approx \Phi_\mathrm{p} \boldsymbol{\eta}_\mathrm{p}(t). \tag{6}$$

Here, the primary eigenmodes $\boldsymbol{\eta}_\mathrm{p}(t) \in \mathbb{R}^{n_\mathrm{p}}$ with the lowest magnitude eigenvalue and therefore lowest frequency are chosen. With the transformation (6) and by left-multiplying (1) with $\Phi_\mathrm{p}^\mathrm{T}$, we obtain the structural dynamics in modal coordinates

$$\ddot{\boldsymbol{\eta}}_\mathrm{p}(t) + D^* \dot{\boldsymbol{\eta}}_\mathrm{p}(t) + K^* \boldsymbol{\eta}_\mathrm{p}(t) = F_u^* \boldsymbol{u}(t), \quad t < 0. \tag{7}$$

Table 1. Geometry and Material Parameters.

Description	Formula sign	Value	Unit
Density	ρ	7850	$\mathrm{kg/m^3}$
Young's modulus	E	210×10^9	$\mathrm{N/m^2}$
Poisson's ratio	ν	0.3	
Vertical columns, quadratic hollow profiles			
Length	L_v	3	m
Width	w_v	0.3	m
Wall thickness	t_v	0.01	m
Horizontal links, rectangular hollow profiles			
Length	L_h	4.75	m
Width	w_h	0.504	m
Height	h_h	0.12	m
Wall thickness	t_h	0.008	m
Horizontal diagonal links			
Length	L_hd	6.72	m
Width	w_hd	0.01	m
Height	h_hd	0.06	m
Diagonal links			
Length	L_vd	10.18	m
Width	w_vd	0.15	m
Height	h_vd	0.012	m

Here, $D^* = \Phi_\mathrm{p}^\mathrm{T} D \Phi_\mathrm{p}$ is the modal damping matrix, K^* is the diagonal matrix of squared eigenvalues and $F_u^* = \Phi_\mathrm{p}^\mathrm{T} \boldsymbol{F}_u$ the transformed input matrix.

For simulation purposes and the application of control engineering methods, (7) is converted to a state space representation. By choosing the state vector as $\boldsymbol{x}(t) = \left[\boldsymbol{\eta}_\mathrm{p}(t) \ \dot{\boldsymbol{\eta}}_\mathrm{p}\right]^\mathrm{T}$, we can reformulate the dynamics as

$$\begin{aligned} \dot{\boldsymbol{x}}(t) = \begin{bmatrix} 0 & I \\ -K^* & -D^* \end{bmatrix} \boldsymbol{x}(t) + \begin{bmatrix} 0 \\ F_u^* \end{bmatrix} \boldsymbol{u}(t), \quad t > 0 \\ \boldsymbol{y}(t) = C\boldsymbol{x}(t), \quad \boldsymbol{x}(t=0) = \boldsymbol{x}_0, \end{aligned} \tag{8}$$

where the output matrix $C \in \mathbb{R}^{(m_\mathrm{l}+m_\mathrm{c}) \times 2n_\mathrm{p}}$ maps the state to the quantities measured by strain gauges and cameras.

2.4 Reduced-Order Local Models

As in Warsewa et al. (2019), local models for the structure in Fig. 1 are derived using a combination of two different model order reduction techniques - the system equivalent expansion reduction process (SEREP) and Guyan condensation. The latter is an established static condensation method. For its application, the model's DOFs are divided into a set of active coordinates $\boldsymbol{q}_\mathrm{a}(t)$ and a set of dependent ones $\boldsymbol{q}_\mathrm{d}(t)$ with $\boldsymbol{q}_\mathrm{f}(t) = [\boldsymbol{q}_\mathrm{a}(t) \ \boldsymbol{q}_\mathrm{d}(t)]^\mathrm{T}$. Mass and stiffness matrix are rearranged accordingly

$$M_\mathrm{f} = \begin{bmatrix} M_\mathrm{aa} & M_\mathrm{ad} \\ M_\mathrm{da} & M_\mathrm{dd} \end{bmatrix}, \qquad K_\mathrm{f} = \begin{bmatrix} K_\mathrm{aa} & K_\mathrm{ad} \\ K_\mathrm{da} & K_\mathrm{dd} \end{bmatrix}. \tag{9}$$

For each of the four subsystems shown in Fig.1, its respective DOFs are retained in $\boldsymbol{q}_\mathrm{a}(t)$ while all other DOFs become dependent. The full global state vector $\boldsymbol{q}_\mathrm{f}(t)$ of the whole structure can then be calculated using the Guyan transformation as stated in Guyan (1965)

$$\boldsymbol{q}_\mathrm{f}(t) = \begin{bmatrix} I \\ -K_\mathrm{dd}^{-1} K_\mathrm{da} \end{bmatrix} \boldsymbol{q}_\mathrm{a}(t) = T_\mathrm{G} \boldsymbol{q}_\mathrm{a}(t). \tag{10}$$

As a static technique, Guyan condensation on its own does not allow accurate reproduction of the structural dynamics because inertia terms are neglected in the transformation (10). In the application of the SEREP method, the dynam-

ics are expressed by a reduced set of system eigenmodes $\boldsymbol{\eta}_\mathrm{r} \in \mathbb{R}^{n_\mathrm{r}}$ as obtained from modal analysis in Sec. 2.3 with

$$\boldsymbol{q}_\mathrm{f}(t) = \begin{bmatrix} \boldsymbol{q}_\mathrm{a}(t) \\ \boldsymbol{q}_\mathrm{d}(t) \end{bmatrix} \approx \underbrace{\begin{bmatrix} \Phi_\mathrm{a} \\ \Phi_\mathrm{d} \end{bmatrix}}_{\Phi_\mathrm{r}} \boldsymbol{\eta}_\mathrm{r}(t). \tag{11}$$

A reduced order model in active DOFs $\boldsymbol{q}_\mathrm{a}(t)$ is then obtained using a generalized inverse of Φ_a

$$\boldsymbol{q}_\mathrm{f}(t) \approx \Phi_\mathrm{r} \left[\Phi_\mathrm{a}^\mathrm{T} \Phi_\mathrm{a}\right]^{-1} \Phi_\mathrm{a}^\mathrm{T} \boldsymbol{q}_\mathrm{a}(t) = T_\mathrm{U} \boldsymbol{q}_\mathrm{a}(t) \tag{12}$$

according to O'Callahan and Li (1996), where $\Phi_\mathrm{a} \in \mathbb{R}^{n_\mathrm{a} \times n_\mathrm{r}}$ is the matrix of active eigenvectors with n_a the number of active DOFs. The transformations T_G and T_U can be combined to a single one as proposed by Avitabile (2005)

$$T_\mathrm{H} = T_\mathrm{G} + (T_\mathrm{G} - T_\mathrm{U}) \left[\Phi_\mathrm{a} \Phi_\mathrm{a}^\mathrm{T} T_\mathrm{U}^\mathrm{T} M_\mathrm{f} T_\mathrm{U}\right] \tag{13}$$

which is known as the SEREP-Guyan transformation. For each subsystem s, with $s \in \{1, 2, 3, 4\}$, a transformation $T_{\mathrm{H}s}$ is obtained that projects from the local coordinates $\boldsymbol{q}_s(t)$ to the global state. The local dynamics for each subsystem s are obtained by left-multiplying (1) with the transpose of $T_{\mathrm{H}s}$

$$M_s \ddot{\boldsymbol{q}}_s(t) + D_s \dot{\boldsymbol{q}}_s(t) + K_s \boldsymbol{q}_s(t) = F_{us} \boldsymbol{u}_s(t), \quad t > 0. \tag{14}$$

Here, $\boldsymbol{u}_s(t)$ are the inputs corresponding to the actuators present in subsystems s. The fourth module does not have any input. For the following application of control engineering methods, further model order reduction by means of modal analysis is performed on the local systems. This allows e. g. the execution of observers and controllers in real-time on low-cost hardware which is desirable for decentralized systems. We apply the method described in Sec. 2.3 to the local dynamics (14) to approximate $\boldsymbol{q}_s(t)$ by a small number of eigenmodes $\boldsymbol{\eta}_s(t) \in \mathbb{R}^{n_s}$

$$\boldsymbol{q}_s(t) \approx \Phi_s \boldsymbol{\eta}_s(t). \tag{15}$$

The reduced order local dynamics are then given as

$$\ddot{\boldsymbol{\eta}}_s(t) + D_s^* \dot{\boldsymbol{\eta}}_s(t) + K_s^* \boldsymbol{\eta}_s(t) = F_{us}^* \boldsymbol{u}_s(t), \quad t > 0. \tag{16}$$

By choosing the local state vector as $\boldsymbol{x}_s = [\boldsymbol{\eta}_s \ \dot{\boldsymbol{\eta}}_s]^\mathrm{T}$, the subsystem dynamics can be formulated in state space

$$\begin{aligned} \dot{\boldsymbol{x}}_s(t) &= \underbrace{\begin{bmatrix} 0 & I \\ -K_s^* & -D_s^* \end{bmatrix}}_{A_s} \boldsymbol{x}_s(t) + \underbrace{\begin{bmatrix} 0 \\ F_{us}^* \end{bmatrix}}_{B_s} \boldsymbol{u}_s^*(t) \\ \boldsymbol{y}_s(t) &= C_s \boldsymbol{x}_s(t), \quad \boldsymbol{x}_s(t=0) = \boldsymbol{x}_{s0}. \end{aligned} \tag{17}$$

The local output mapping C_s yields the full camera output but only the length measurements from strain gauges on elements contained in subsystem s. It is given by

$$C_s = \begin{bmatrix} C_{\mathrm{len},s} & 0 \\ C_{\mathrm{cam,f}} & 0 \end{bmatrix} \underbrace{\begin{bmatrix} T_{\mathrm{H}s} \Phi_s & 0 \\ 0 & T_{\mathrm{H}s} \Phi_s \end{bmatrix}}_{L_s^\mathrm{T}}, \tag{18}$$

with the local element length mapping $C_{\mathrm{len},s} \in \mathbb{R}^{m_s \times n_s}$, where m_s is the number of strain gauge sensors available in the module. The tranformation L_s relates $\boldsymbol{x}_s$ to the global state vector $\boldsymbol{x}_\mathrm{f} = [\boldsymbol{q}_\mathrm{f} \ \dot{\boldsymbol{q}}_\mathrm{f}]^\mathrm{T}$.

3. STATE ESTIMATION

In the following, decentralized and distributed state estimation with discrete time Kalman filters is conducted for the local subsystem dynamics presented in Sec. 2.4. To compare the performance of the distributed observers to a centralized approach, a centralized observer is briefly introduced in the subsequent section.

3.1 Distributed Observers

Given the discrete time equivalents F_s and G_s of the system matrix A_s and input mapping B_s from (17) according to Simon (2006), the prediction step of a local Kalman filter can be formulated as

$$\begin{aligned} \hat{\boldsymbol{x}}_s^-[k] &= F_s \hat{\boldsymbol{x}}_s^+[k-1] + G_s \boldsymbol{u}_s[k-1] \\ P_s^-[k] &= F_s P_s^+[k-1] F_s^\mathrm{T} + Q_s, \end{aligned} \tag{19}$$

where $\hat{\boldsymbol{x}}_s^-[k]$ is the *a priori* state estimate at step k before the processing of measurements, $\hat{\boldsymbol{x}}_s^+[k-1]$ the *a posteriori* estimate after measurement incorporation from the previous filter iteration and $P_s^-[k]$ and $P_s^+[k-1]$ are the corresponding estimation error covariances. The system noise covariance for each substructure is obtained from the global system noise covariance $Q_\mathrm{o} = I^{n \times n} \cdot q_\mathrm{o}$ according to

$$Q_s = L_s Q_\mathrm{o} L_s^\mathrm{T}, \tag{20}$$

with L_s from Eq. (18). Given a vector of measurement signals $\boldsymbol{y}_s[k]$ for the current time step, the *a priori* estimate and error covariance are updated in a correction step according to

$$\begin{aligned} \hat{\boldsymbol{x}}_s^+[k] &= \hat{\boldsymbol{x}}_s^-[k] + K_s[k] \left(\boldsymbol{y}_s[k] - C_s \hat{\boldsymbol{x}}_s^-[k]\right) \\ P_s^+[k] &= \left(I - K_s[k] C_s\right) P_s^-[k], \end{aligned} \tag{21}$$

where the Kalman gain $K_s[k]$ is given as

$$K_s[k] = P_s^-[k] C_s^\mathrm{T} \left[C_s P_s^-[k] C_s^\mathrm{T} + R_s\right]^{-1}. \tag{22}$$

Here, R_s is the measurement noise covariance. The noise on individual signals is assumed uncorrelated such that R_s can be expressed as

$$R_s = \begin{bmatrix} I^{m_s \times m_s} \cdot r_\mathrm{l} & 0 \\ 0 & I^{m_\mathrm{c} \times m_\mathrm{c}} \cdot r_\mathrm{c} \end{bmatrix} \tag{23}$$

with the strain gauge noise variance r_l and the camera signal noise variance r_c.

3.2 Centralized Estimation

For centralized state observation a reduced order model (8) obtained by modal analysis with $n_\mathrm{p} = 10$ smallest magnitude primary eigenmodes is used. The discrete time Kalman filter equations are the same as above except that the centralized observer uses all available measurements in the correction step and a global system model.

4. CONTROL DESIGN

In this section, a decentralized control algorithm is introduced such that each module is controlled separately, based on the models in Sec. 2.4 and using the actuators installed in the respective subsystem.

4.1 Decentralized Control

An optimal state feedback controller is designed by means of the LQR algorithm. The states for feedback are obtained from the distributed Kalman filters introduced in Sec.3.1. The control law yields

$$\boldsymbol{u}_s[k] = K_{\mathrm{lqr},s}(\hat{\boldsymbol{x}}_s^+[k] - \boldsymbol{x}_{\mathrm{d},s}), \tag{24}$$

Table 2. Simulation Parameters.

Symbol	Value	Unit	Description
T_s	0.001	s	system sample time
T_d	0.01	s	filter/controller sample time
n_p	186		# modes system
n_r	10		# modes SEREP
n_s	10		# modes local models
α_1	0.05		damping coefficients
α_2	0.001		
σ_c	4×10^{-6}	m^2	camera noise variance
σ_l	1×10^{-8}	m^2	strain gauge noise variance
q_o, q_s	1		system noise covariance
r_c	1×10^{-6}	m^2	camera noise covariance
r_l	1×10^{-9}	m^2	strain gauge noise covariance
q_c	2×10^6		state cost weight LQR

where $K_{\mathrm{lqr},s} \in \mathbb{R}^{n_{u,s} \times n_s}$ is the state feedback matrix for subsystem s and $\boldsymbol{x}_{\mathrm{d},s}$ is the desired state, i. e. zero displacement and velocity. The feedback matrix is determined such that the cost function

$$J = \sum_{k=0}^{\infty} (\hat{\boldsymbol{x}}_s^+[k])^\mathrm{T} Q_\mathrm{c} \hat{\boldsymbol{x}}_s^+[k] + (\boldsymbol{u}_s[k])^\mathrm{T} R_\mathrm{c} \boldsymbol{u}_s[k] \qquad (25)$$

is minimal for given weighting matrices $Q_\mathrm{c} = I^{n_s \times n_s} \cdot q_c$ and $R_\mathrm{c} = I^{n_{u,s} \times n_{u,s}}$.

4.2 Centralized Control

To evaluate the performance of the decentralized controller, a centralized LQG is designed for comparison. This controller follows the same equations as the decentralized one in Sec. 4.1 while using the global model of the centralized Kalman filter in Sec. 3.2 and accessing all actuators.

5. RESULTS

To assess the performance of the decentralized control method presented in this contribution, we investigate the dynamic response of the structure in Fig. 1 for an initial displacement in x-direction in the controlled and uncontrolled case. Performance of the decentralized observers and controllers is compared to the centralized approaches by depicting the x-displacement of node 47, the node highlighted in pink in Fig. 1. This node is chosen because no camera measurements are available on this floor and the displacements are higher in upper stories. In the simulations, the structural dynamics are represented by (8) with the first $n_\mathrm{p} = 186$ eigenmodes for which the eigenfrequencies are below the Nyquist frequency for a sample time of $T_\mathrm{s} = 0.001\,\mathrm{s}$. These and other simulation parameters, including controller/observer settings and noise variance values are summarized in Tab. 2.

5.1 Performance of Decentralized vs. Centralized Approach

In Fig. 2, the x-displacement of node 47 is plotted together with the estimated values. While the central observer accurately tracks the actual displacement value almost immediately, the decentralized observer in the fourth module takes about 0.25 s to converge. Afterward, the local estimate is hardly distinguishable from the global one. The slightly lower performance of the decentralized filters is not surprising and an acceptable tradeoff since they are not using the sensor data from the other modules.

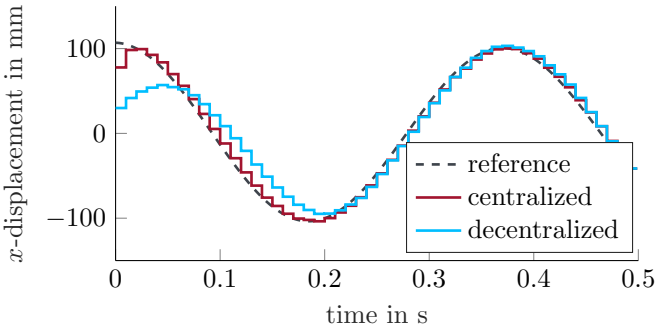

Fig. 2. Centralized and decentralized estimation of the x-displacement of node 47 for an initial displacement of the structure.

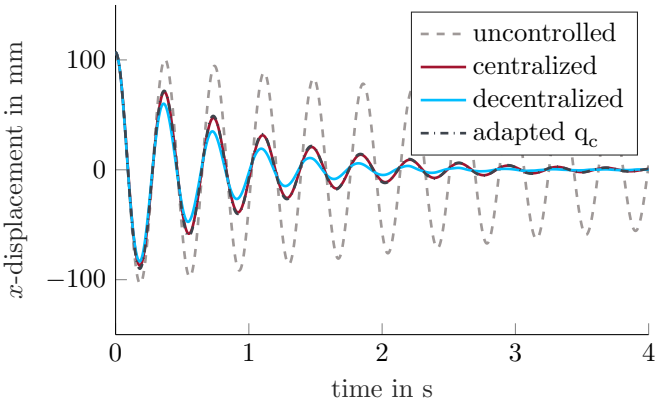

Fig. 3. Centralized and decentralized control for an initial displacement of the structure. The x-displacement of node 47 is shown.

Using the state estimates of the decentralized observers in the lower three modules, the corresponding decentralized controllers damp structural oscillations. Again, the decentralized approach is compared to the centralized one and the respective performance is shown in Fig. 3. In the uncontrolled case, oscillations up to an amplitude of about 60 mm are still visible after 4 s. Both control approaches manage to damp the structural vibration significantly in the considered time interval with almost zero residual oscillation. However, the local controllers (blue) achieve quicker damping of the oscillations caused by the initial displacement of the structure. At first, the state-cost weights q_c for the controllers in each actuated module were set to the same value as for the centralized LQR (see Tab. 2). When each local LQR is assigned a state-cost weight of $q_c = 1 \times 10^6$ (dash-dotted dark line), almost identical damping performance results. This can be attributed to the different accuracy of local dynamic models when compared to a global reduced order model.

5.2 Energy Demand

To further explore the differences between decentralized and centralized control, we examine the energy consumption of both approaches. Here, the expended power is calculated by multiplying the actuator forces with the element length change velocities of the corresponding trusses and taking the resulting product's absolute value. Summing up the individual power terms and integrating over

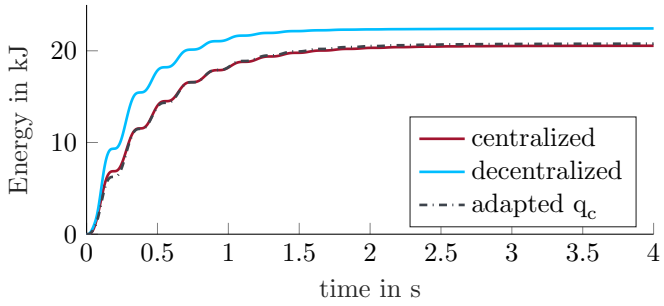

Fig. 4. Energy consumption of centralized and decentralized control.

time yields the results depicted in Fig. 4. We observe, that the decentralized controllers consume about 10 % more energy than the centralized LQG with the initial value of q_c. When the state-cost weight of the local controllers is adjusted, almost identical controller performance is observed in Fig. 3. In Fig. 4 we see, that the same applies to the energy demand. Minor differences are visible, but they are not significant. With the local LQRs it is also possible to choose different controller parameters in each module or to adapt them over time. For a more in-depth assessment of both control performance and energy demand, various load scenarios as well as different parameters for Kalman filters and LQR controllers need to be considered.

5.3 Robustness Analysis

As stated e. g. by Doyle (1978), stability with respect to model parameter uncertainties cannot be guaranteed for LQG control approaches. In order to analyze the robustness of the presented decentralized control approach on that account, Monte Carlo simulations were conducted with varying model parameters. In a first simulation experiment, the structure's parameters in Tab. 1 (except for element lengths) and the damping coefficients were assumed to follow a normal distribution. A standard deviation of $\sigma = 5\,\%$ of the nominal value was assumed for each parameter. A second simulation study was conducted, where the eigenvalues ω_i of the simulation model (8) were assumed normally distributed instead. In this experiment, a higher standard deviation of $\sigma = 10\,\%$ of the nominal value was chosen. The number of simulation runs in each experiment was $N = 10000$.

Results for the first experiment are depicted in Fig. 5 a) with the worst and best result highlighted respectively. For ease of comparison, the damping behavior is illustrated for node 47 – as previously done in Figs. 2 and 3. We observe a stable response of the decentralized controllers for all tested parameter sets. The centralized LQG control was also tested for the same parameter sets and proved stable in all but two simulation runs (not shown).

When the structure's eigenvalues are varied instead (assuming no changes in mode shapes), a different outcome is observed in Fig. 5 b). Stability of the decentralized LQG controllers cannot be guaranteed as unstable behavior is observed for many samples. Here, the centralized LQG is, however, stable in all cases (also not shown). A standard deviation of $\sigma = 10\,\%$ leads to quite high uncertainty which might not be realistic in practice. It still shows the limits of the proposed control scheme and the importance of good agreement between the modeled and the actual eigenvalues of the structure.

Given deviation from the nominal parameters of the structure is in the range of $\pm 5\,\%$, the decentralized control approach is assumed to be stable. This needs to be confirmed in practical application or with more involved simulation studies.

6. CONCLUSION

In this contribution, we introduced a method for decentralized state estimation and control design for adaptive structures. Based on previous work, models for local subsystems were derived from a finite element model by means of SEREP-Guyan reduction followed by subsequent modal analysis. Here, we have shown the applicability of this method to perform decentralized control of a sample adaptive structure. Information on the structural deformation is obtained from a limited number of strain gauges and a camera system. LQG control was employed for each subsystem independently. As opposed to existing work, our approach neither requires the communication of states nor the introduction of coupling forces and their estimation because the approximated global dynamics are preserved in the local models.

Both the performance and the energy demand of the decentralized controllers were found to be comparable to a centralized reference. In a practical application, the benefits of decentralization – higher redundancy and cost-effective realization – can thus be achieved without sacrificing performance. In simulation studies, the stability of the decentralized LQG controllers was confirmed if the model parameters do not deviate more than $\pm 5\,\%$ from the nominal values used to construct the dynamical simulation model. Care must be taken to guarantee good matching between modeled and actual eigenvalues when using a reduced number of eigenmodes to reproduce structural dynamics.

In further work, we wish to transfer this methodology to different structures (taller building in particular) where we also want to take communication between local modules into account.

ACKNOWLEDGEMENTS

The authors gratefully acknowledge the generous funding of this work by the German Research Foundation (DFG - Deutsche Forschungsgemeinschaft) as part of the Collaborative Research Center 1244 (SFB) “Adaptive Skins and Structures for the Built Environment of Tomorrow” / projects B02 and B04.

REFERENCES

Avitabile, P. (2005). Model reduction and model expansion and their applications–part 1 theory. In *Proceedings of the Twenty-Third International Modal Analysis Conference, Orlando, FL, USA*.

Bakule, L., Rehák, B., and Papík, M. (2016). Decentralized networked control of building structures. *Computer-Aided Civil and Infrastructure Engineering*, 31(11), 871–886.

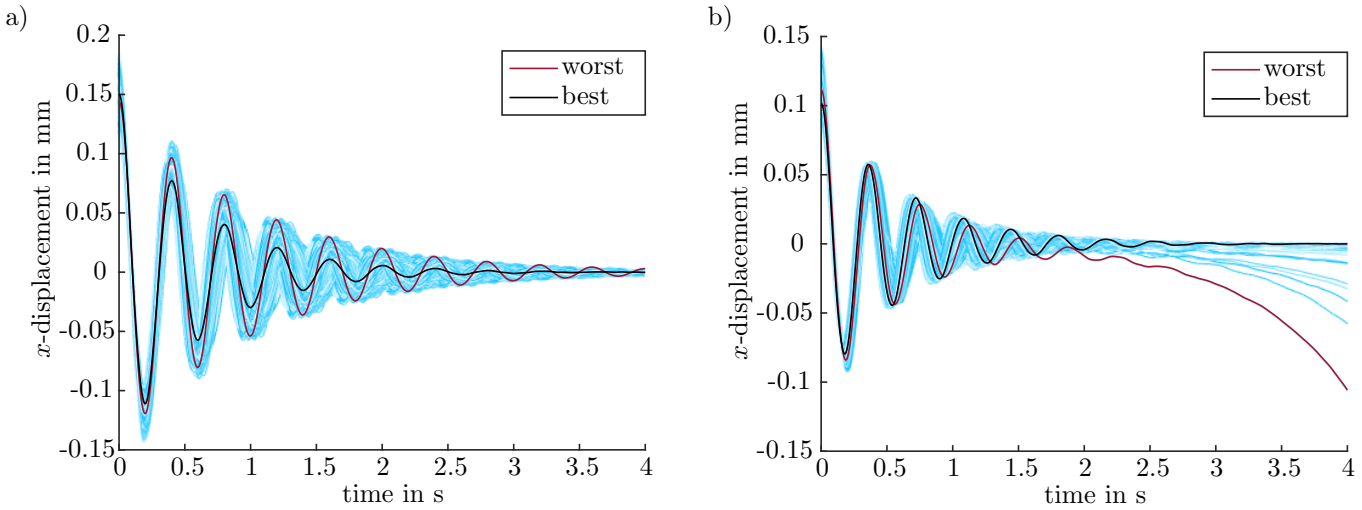

Fig. 5. Monte Carlo simulations of the decentralized control approach with $N = 10000$ samples shown for node 47. a) Normally distributed model parameters ($\sigma = 5\,\%$); b) Normally distributed eigenvalues ($\sigma = 10\,\%$).

Doyle, J.C. (1978). Guaranteed margins for LQG regulators. *IEEE Transactions on automatic Control*, 23(4), 756–757.

Gawronski, W. (2004). *Advanced structural dynamics and active control of structures*. Springer Science & Business Media.

Guerra, F., Hartlieb, S., Warsewa, A., Haist, T., Osten, W., and Sawodny, O. (2019). Deformation measurement of large buildings by holographical point replication. In *Optics for Arts, Architecture, and Archaeology VII*, volume 11058, 110580G. International Society for Optics and Photonics.

Guyan, R.J. (1965). Reduction of stiffness and mass matrices. *AIAA journal*, 3(2), 380–380.

Heidingsfeld, M., Rapp, P., Böhm, M., and Sawodny, O. (2017). Gramian-based actuator placement with spillover reduction for active damping of adaptive structures. In *2017 IEEE International Conference on Advanced Intelligent Mechatronics (AIM)*, 904–909. IEEE.

Lei, Y., Wu, D.T., and Lin, Y. (2012). A decentralized control algorithm for large-scale building structures. *Computer-Aided Civil and Infrastructure Engineering*, 27(1), 2–13.

Lynch, J.P. and Law, K.H. (2002). Decentralized control techniques for large-scale civil structural systems. In *Proc. of the 20th Int. Modal Analysis Conference (IMAC XX)*.

O'Callahan, J. and Li, P. (1996). SEREP expansion. In *Proceedings of the 14th International Modal Analysis Conference*, volume 2768, 1258.

Rapp, P., Heidingsfeld, M., Böhm, M., Sawodny, O., and Tarín, C. (2017). Multimodal sensor fusion of inertial, strain, and distance data for state estimation of adaptive structures using particle filtering. In *2017 IEEE International Conference on Advanced Intelligent Mechatronics (AIM)*, 921–928. IEEE.

Rofooei, F.R. and Monajemi-Nezhad, S. (2006). Decentralized control of tall buildings. *The Structural Design of Tall and Special Buildings*, 15(2), 153–170.

Sandell, N., Varaiya, P., Athans, M., and Safonov, M. (1978). Survey of decentralized control methods for large scale systems. *IEEE Transactions on automatic Control*, 23(2), 108–128.

Siljak, D.D. (2011). *Decentralized control of complex systems*. Courier Corporation.

Simon, D. (2006). *Optimal state estimation: Kalman, H infinity, and nonlinear approaches*. John Wiley & Sons.

Sobek, W. and Teuffel, P. (2001). Adaptive systems in architecture and structural engineering. In *Smart Structures and Materials 2001: Smart Systems for Bridges, Structures, and Highways*, volume 4330, 36–46. International Society for Optics and Photonics.

Spencer, B.F. and Nagarajaiah, S. (2003). State of the art of structural control. *Journal of structural engineering*, 129(7), 845–856.

Su, T.J., Aabuska, V., and Raig, R.R. (1995). Substructure-based controller design method for flexible structures. *Journal of Guidance, Control, and Dynamics*, 18(5), 1053–1061.

Wagner, J.L., Gade, J., Heidingsfeld, M., Geiger, F., von Scheven, M., Böhm, M., Bischoff, M., and Sawodny, O. (2018). On steady-state disturbance compensability for actuator placement in adaptive structures. *at-Automatisierungstechnik*, 66(8), 591–603.

Warsewa, A., Böhm, M., Rapp, P., Sawodny, O., and Tarín, C. (2019). Decentralized and Distributed Observer Design for Large-Scale Structures using Dynamic Condensation. In *2019 IEEE 15th International Conference on Automation Science and Engineering (CASE)*, 1256–1262. doi:10.1109/COASE.2019.8843266.